metals

MDPI

Article

Practical Approbation of Thermodynamic Criteria for the Consolidation of Bimetallic and Functionally Gradient Materials

Alexander Khaimovich [1], Yaroslav Erisov [2,3,*], Anton Agapovichev [1], Igor Shishkovsky [4], Vitaliy Smelov [1] and Vasilii Razzhivin [2,3]

1 Engine Production Technology Department, Samara National Research University, 34 Moskovskoye Shosse, 443086 Samara, Russia; berill_samara@bk.ru (A.K.); agapovichev5@mail.ru (A.A.); pdla_smelov@mail.ru (V.S.)
2 Metal Forming Department, Samara National Research University, 34 Moskovskoye Shosse, 334086 Samara, Russia; vasia.razzhivin@yandex.ru
3 Samara Federal Research Center of the Russian Academy of Sciences, 3A Studencheskiy Pereulok, 443001 Samara, Russia
4 Center for Design, Manufacturing and Materials, Skoltech, Skolkovo Institute of Science and Technology Bolshoy Boulevard 30, Bld. 1, 121205 Moscow, Russia; shishkowsky@gmail.com
* Correspondence: yaroslav.erisov@mail.ru

Abstract: This study concerns the key problem of determining the conditions for the consolidation or fracture of bimetallic compounds and high-gradient materials with different coefficients of thermal expansion. The well-known approach to determining the strength is based on the assessment of the critical energy release rates during fracture, depending on the conditions of loading (the portion of shear loading). Unfortunately, most of the experimental results cannot be used directly to select suitable fracture toughness criteria before such a connection is made. This especially applies to the region of interphase interaction, when it is required to estimate the internal energy of destruction accumulated during the preparation of the joint in the adhesion layer within the range of 20–50 μm. Hence, criteria for the adhesive consolidation of bimetallic compound layers were obtained on the basis of the thermodynamics of nonequilibrium processes. The analysis of the quality of the joint using the obtained criteria was carried out on the basis of the calculation of isochoric and isobaric heat capacities and coefficients of thermal expansion of multiphase layers. The applicability of the criteria for the qualitative assessment of the adhesion of layers is demonstrated in the example of bimetallic joints of steel 316L—aluminum alloy AlSi10Mg obtained by the SLM method at various fusion modes.

Keywords: selective laser melting (SLM); laser-controlled reaction synthesis; functional graded (FG) intermetallic structures; functional bimetallic materials (FBM); thermodynamical approach; adhesive consolidation criteria; 316L; AlSi10Mg

Citation: Khaimovich, A.; Erisov, Y.; Agapovichev, A.; Shishkovsky, I.; Smelov, V.; Razzhivin, V. Practical Approbation of Thermodynamic Criteria for the Consolidation of Bimetallic and Functionally Gradient Materials. *Metals* **2021**, *11*, 1960. https://doi.org/10.3390/met11121960

Academic Editor: Ankit Srivastava

Received: 3 November 2021
Accepted: 6 December 2021
Published: 6 December 2021

1. Introduction

Analysis of trends in the modern industry development indicates that an effective solution to the problem of obtaining specific, often incompatible characteristics in materials is the development and creation of composite materials. Among the composite materials, we can distinguish functional-gradient materials.

In a functional-gradient material (FGM), both the composition and the structure gradually change in volume, which leads to corresponding changes in the properties of the material [1,2]. A fairly complete overview of modern trends in the creation of FGM can be found in the works [3].

In the case of a sharp difference between the chemical compositions of the FGM phases, one can speak of functional bimetallic materials. The concept of functional bimetallic

materials (FBM) was proposed in 1984 in Japan as a means of obtaining materials for a thermal barrier [4]. FBM is an advanced material that can achieve a transition gradient or sudden transition from one material to another for various materials [2]. In the early stages of FBM production, welding was the main technology for combining dissimilar metals [5], explosive welding [6,7] and laser welding [8] were particularly successful. Among other technologies, laser additive manufacturing is an ideal technology for producing FBM [8].

Functional graded structures (FGS) are another type of composite materials that occupy an intermediate position between FGM and FBM. In the study [9], based on the analysis of technologies for building FGS, two methods of their production from CrNi and Al-powders using additive technologies are compared; these are direct metal deposition (DMD) and selective laser melting (SLM), as presented in Figure 1.

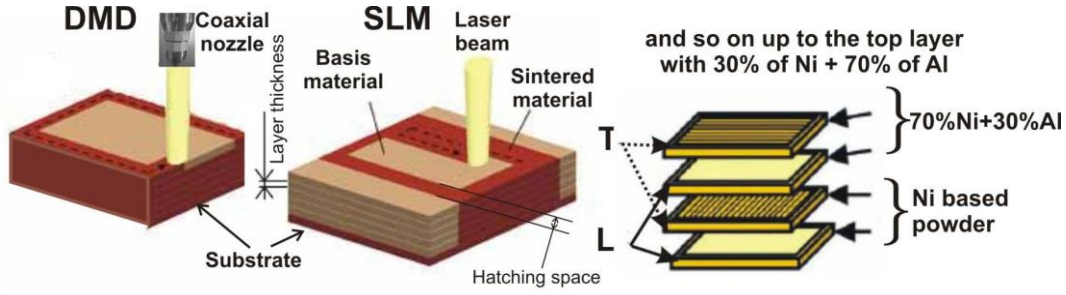

Figure 1. Obtaining the Functional graded structures by DMD иSLM methods Schematic of the multicomponent-graded structure fabrication by the DMD and SLM processes. Longitudinal, L; transversal, T [9].

The LDMD method for FGS manufacturing is schematically presented in Figure 1 and was proposed earlier [10]. The layers were formed from Ni (Diamaloy) and Al based powders on a related substrate according to the following strategy: the first two layers were pure NiCr, the next two were 70% of NiCr + 30% of Al, the third pair of layers was 50% of NiCr + 50% of Al, and finally the upper 7th and 8th layers had a ratio of 30% of NiCr + 70% of Al. For the Fe-Al system, such a system was successfully tested in [11].

FBM and FGS-materials must have strong interlayer bonds, which are preserved during further technological processing and under operating conditions. It is assumed that the material retains its macroscopic continuity up to the initiation of an interphase crack. Delamination is considered as a process of initiation and development of continuity microdefects, leading to the formation of interlayer cracks. Delamination is formed due to a combination of two or three main delamination mechanisms (modes): normal opening mode I (a), sliding shear mode II (b), and scissor shear mode III (c) [6,12]. There are numerous models of damage mechanics within the framework of the phenomenological approach [13–16], which are applicable for a monolithic material and separate components of layered materials; most of them do not allow assessment of the fracture in the joint zone, as they do not take into consideration the inhomogeneity of thermomechanical properties between different phases interfaces.

It should be mentioned that materials with poor thermal conductivity obtained by fused layer deposition of metal powder are prone to cracking. The first reason for the occurrence of cracks is an increased level of residual stresses, which are formed due to uneven heating during the synthesis of layers, during which the upper layers undergo significant tensile stresses during solidification [9]. The presence of a certain number of pores and structural defects, from which the development of cracks begins, is the second reason for the tendency to crack formation. Fundamental criteria for the initiation and propagation of fracture can be obtained using the concept of energy balance at the crack front, which, for an equilibrium crack, can be expressed as the equality of the available energy and the energy required to create a unit area of the new crack surface [17].

Failure analysis is often used during the design phase of composite structures, which requires accurate and reliable determination of material properties. For adhesive joints,

these properties are strength parameters and critical energy release (CERR) rate, which is characterized by the toughness of the material. In this case, CERR is the most defining parameter [12]. It is advisable to determine the criteria that allow one to find CERR as a function of the ratio of modes of the involved separation mechanisms (I, II, III). A number of studies have been devoted to this issue [12,18,19]. It should also be noted that the cohesion law [12,20], which is based on the universal law of binding energy proposed by Rose et al., is applicable to the interface of the bimetallic material [21]. Most macroscopic fracture theories are based on the principles of solid mechanics and classical thermodynamics [1]. With regard to additive technologies, the existing energy approaches can be expanded if we consider the conditions for the consolidation of a multiphase material, in particular FBM, from the point of view of the thermodynamics of nonequilibrium processes.

2. Theoretical Foundations of the Research Method

The process of additive synthesis of FBM is high-temperature, and energy exchange in a local volume at the interface boundary of a bimetallic compound can be so intense that separation is possible. The purpose of this study is to identify the conditions for the consolidation of phases of a multiphase medium with different thermophysical properties characteristic of bimetallic materials, from the conditions of the balance of the thermal and stress-strain states, as well as phase equilibrium in the interface. Consolidation in this context means the absence of interphase separation under conditions of thermodynamic equilibrium. In this regard, to solve the key problem of finding conditions for the consolidation of a multiphase material from the point of view of thermodynamics, the heat transfer equation at the interface was considered, reflecting the interphase mechanical interaction.

Modeling of the bimetallic compound interface was carried out on the basis of the state analysis determined by the thermodynamics of irreversible processes. A similar approach at the macrolevel was used in [22] in relation to a medium consisting of deformable grains. All macroscopic processes in a heterogeneous medium were considered by the methods of continuum mechanics using averaged or macroscopic parameters.

As a result, it was possible to obtain the criteria for the consolidation of two phases K_1 and K_2, dependences (1) and (2), which can be considered as necessary conditions for the formation of a stable adhesive bond from the point of view of thermodynamics:

$$K_1 = \frac{\left(1 - \frac{s_\Omega^v}{s_\Omega^w}\right)k^w}{\left(1 - \frac{s_\sigma^v}{s_\sigma^w}\right)k^v} \to 1, \tag{1}$$

$$K_2 = \frac{(1 - k^v)\alpha_t^w}{(1 - k^w)\alpha_t^v} \to 1, \tag{2}$$

where c_Ω^v, c_Ω^w are the molar isochoric heat capacities of layers v and w, c_σ^v, c_σ^w are the molar isobaric heat capacity of the layers, α^v, α^w are the linear coefficients of thermal expansion, and $k^v = s_\Omega^v / s_\sigma^v$, $k^w = s_\Omega^w / s_\sigma^w$ are the coefficients inverse to the polytropic indicator.

To find criteria (1) and (2) at the interface boundary, an analytical method was used to determine all thermodynamic quantities included in them. Isobaric and isochoric heat capacities of a pure substance from the composition of each phase were calculated according to Debye's law of molar heat capacity [23]:

$$s_\Omega = 3R\left[12\left(\frac{T}{\theta}\right)^3 \int_0^{T/\theta} \frac{x^3}{e^x - 1}dx - \frac{3T/\theta}{e^{T/\theta} - 1}\right], \tag{3}$$

where θ is the Debye's temperature, which is defined as

$$\theta = \frac{\hbar\nu}{k}. \tag{4}$$

In Equations (3) and (4), $\hbar$ is Planck's constant, k is Boltzmann's constant, ν is the vibration frequency of atoms, x is the parameter, determined on the basis of the solid-state theory [23], and T is temperature (all calculations are made for room temperature, T = 298 K). The characteristic Debye temperatures of substances are known from literature, for example, [24].

Equation (1) is valid when determining the Debye temperature for a pure substance, and for a substance in a compound (as part of a phase), the Debye temperature is calculated using the Koref's equation [24]. According to Koref's rule, data on the melting points of a compound, and melting points and Debye temperatures of pure substances outside the compound, make it possible to obtain the melting temperatures of these substances in a compound, according to the dependence:

$$\theta^* = \theta\sqrt{\frac{T_m^*}{T_m}}. \tag{5}$$

Here θ^*, θ are the characteristic Debye temperatures of the element in the compound, with other elements of phase and the element outside the compound of phase, and T_m^*, T_m are the melting temperatures of the entire phase and the element outside the compound of the phase. The isochoric heat capacity (s_Ω) values are determined from θ^* using the Debye's equation separately for each phase component. Then, summing them up according to the Neumann-Kopp rule, the isochoric heat capacity of the compound is determined. For the $A_lB_mD_k$ compound, the isochoric heat capacity can be found from the dependence [24,25]:

$$c_\Omega(A_lB_mD_k) = l \cdot s_\Omega(A) + m \cdot s_\Omega(B) + k \cdot s_\Omega(D). \tag{6}$$

The recalculation of the isochoric heat capacity to the isobaric heat capacity was carried out according to the Magnus-Lindemann equation [24]:

$$\begin{array}{c} c_\sigma = c_\Omega + \beta T^{3/2}, \\ \beta = 6.076\frac{n}{(T_m^*)^{3/2}}, \end{array} \tag{7}$$

where n is the number of atoms in the compound ($n = l + m + k$), and T_m^* is the melting point of $A_lB_mD_k$.

The usual approach to assessing the properties of an FGM material is to apply the rule of mixtures. Although these are not really physical or mathematical rules, these relationships can be used to approximate the thermal or mechanical properties of a composite material in terms of individual properties and relative amounts of components. The simplest is the classical linear rule of mixtures (Voigt's estimate) for two constituent materials, based on the assumption of uniform strain or stress of the composite structure [1]. The upper Voigt bound [26,27] for the effective coefficient of thermal expansion α is provided by the expression:

$$\alpha = \frac{\langle E\alpha \rangle}{\langle E \rangle} = \frac{C_1\alpha_1E_1 + C_2\alpha_2E_2}{C_1E_1 + C_2E_2}, \tag{8}$$

where C_1, α_1, E_1 are the volumetric concentration, coefficient of thermal expansion (CTE), and modulus of elasticity related to the first component (phase) of the composite substance, C_2, α_2, E_2, to the second component.

According to [1], two-phase composite material dependences for calculating the CTE are more accurately and experimentally confirmed in works [28–32].

3. Materials and Methods

To determine the applicability of thermodynamic criteria for the consolidation of phases (layers) of a bimetallic material (1) and (2) for the analysis of delamination, a series of experiments was carried out to create a bimetallic compound AlSi10Mg, steel 316L, by the method of selective laser alloying [33]. Due to the different specific energy of

fusion supplied to the surfacing area with a change in the scanning speed, we achieved a different level of mixing of the phase components in the region of formation of the interlayer interface. The elemental composition of the interface was determined by energy dispersive analysis. Thermodynamic consolidation criteria were calculated for each sample. Bimetallic samples were subjected to mechanical testing to assess the adhesion strength of the interlayer interface. The results of mechanical tests were compared with the calculated value of the thermodynamic criterion for phase consolidation.

For the surfacing material, we used powder of aluminum alloy AlSi10Mg. The results of X-ray microscopy study of the morphology and chemical composition of the powder are presented in Table 1. Fusing of aluminum powder was carried out on a pre-cleaned substrate: a plate of steel 316L 2.0 mm thick with the chemical composition, as presented in Table 2.

Table 1. The results of the analysis of the elemental composition of the powder of the aluminum alloy AlSi10Mg.

Mass Fraction of Elements. %				
Al	**Si**	**C**	**O**	**Mg**
81.83	10.73	3.35	2.41	1.30

Table 2. Chemical composition of the substrate material ASTM 316L.

Mass Fraction of Elements. %									
C	**Mn**	P	**S**	**Si**	**Cr**	**Ni**	**Mo**	**Ti**	**Fe**
<0.07	<2.0	<0.045	<0.03	<1.0	16.0–18.0	10.0–14.0	2.0–3.0	<0.5	Other

Fusing of layers of aluminum powder was carried out on an SLM 280 installation in strips 70 × 15 mm in size. Up to 10 layers were deposited sequentially on 5 strips (samples) using technological scanning parameters (Table 3).

Table 3. Technological parameters of scanning.

Mode No.	Laser Power *P*, W	Scanning Speed *V*, mm/s	Scan Step, mm	Layer Thickness *h*, mm	Energy Density *E*, J/mm^3
1	350	450	0.19	0.05	82
2	350	350	0.19	0.05	105
3	350	250	0.19	0.05	147
4	350	150	0.19	0.05	246
5	350	50	0.19	0.05	737

Analysis of the microstructure of bimetallic samples was carried out on thin sections of cross-section using a Zeiss Axio Vert A1 Mat optical microscope (Carl Zeiss Microscopy GmbH, Jena, Germany): with ×200 and ×500 magnification for each sample. To improve the visibility of the grain boundaries, a gray filter was used in a bright field. The etching of the samples was carried out in a solution of following acids: H_2SO_4-HCl-HNO_3-HF in a proportion of 180-180-120-30 mL, respectively, by immersion for 5 min. The processing of the obtained images of the microstructure was carried out in the specialized software system SIAMS 800. (version 800, OOO "SIAMS", Ekaterinburg, Russia).

To determine the chemical composition, a Phenom ProX electron microscope (Phenom-World, Eindhoven, The Netherlands) was used with an attachment for energy dispersive analysis. The chemical composition was measured at the boundary of two materials with a step of 18–20 μm (5 measurements along and 10 measurements across the boundary), at a magnification of ×1000. The measurement results along the border were averaged and processed by statistical methods.

The mechanical tests were carried out to compare the adhesion strength of the interface zone for all samples. The adhesion strength was determined by comparing the wear resistance of the samples to external influences. The samples were blown with steel microballs with a diameter of up to 0.3 mm and at a speed of up to 50 m/s. During blowing, compressive stresses arise in the AlSi10Mg surface layer, and tensile stresses arise in the interface zone, which contribute to delamination. Blowing was carried out until visible signs of wear appeared on all samples in the form of exfoliated AlSi10Mg particles.

4. Results and Discussion

4.1. Experimental Results

The microstructure of the bimetal boundary is presented in Figure 2. On all samples, three zones can be distinguished that are formed during SLM: a zone of deposited material, a heat-affected zone, and a substrate (from bottom to top). With an increase in the energy density, the depth of the heat-affected zone in the substrate increases from 65–80 microns (modes 1–3) to 120–180 μm (modes 4–5). The thickness of the deposited layer decreases with increasing energy density: mode 1—180–240 μm, 2—120–200 μm, 3—60–100 μm; 4–5—20–40 μm. The microstructure of the interface between the layers of a bimetallic compound is presented in Figure 2.

The distribution of chemical elements along the boundary of the bimetal was determined from the results of energy dispersive analysis. The content of the key elements Fe, Cr, Ni, Al, and Si was measured at a distance of 20 μm on both sides of the interface between the bimetal layers. Measurement values, averaged over five points, are presented in Table 4.

Table 4. Content of elements in the interface area.

Step, μm	Content of Elements, wt%				
	Fe	**Cr**	**Ni**	**Al**	**Si**
SLM scanning mode 1					
20	57.09	14.11	8.27	18.34	2.18
0	37.39	9.54	5.33	43.5	4.25
−20	11.43	2.1	0	80.76	5.71
SLM scanning mode 2					
20	60.08	15.16	8.66	14.19	1.91
0	37.53	9.23	5.5	43.85	3.89
−20	4.86	0	0	87.61	7.53
SLM scanning mode 3					
20	61.87	15.25	8.45	12.78	1.65
0	28.72	6.7	3.25	55.58	5.75
−20	5.84	1.51	0.72	84.83	7.1
SLM scanning mode 4					
20	55.58	13.93	8.54	19.73	2.23
0	47.39	11.34	5.73	31.33	4.21
−20	37.09	9.72	5.15	43.74	4.31
SLM scanning mode 5					
20	69.38	16.75	10.12	2.86	0.89
0	67.35	15.79	10.21	5.91	0.74
−20	62.77	14.91	10.1	10.56	1.67

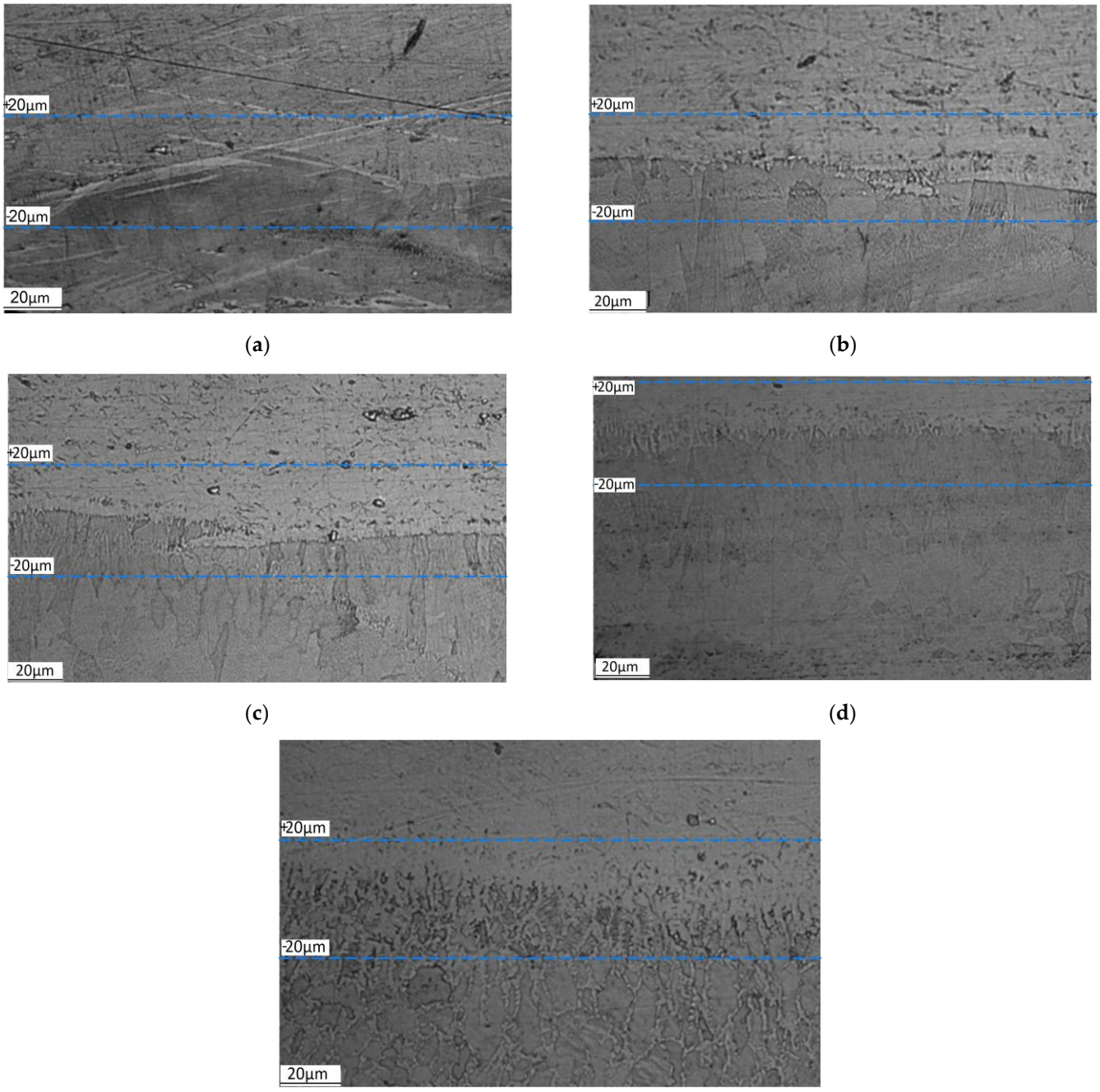

Figure 2. Microstructure of AlSi10Mg—SS316L bimetal interface zone: (**a**) SLM scanning mode 1, (**b**) SLM scanning mode 2, (**c**) SLM scanning mode 3, (**d**) SLM scanning mode 4, and (**e**) SLM scanning mode 5 (from bottom to top: a zone of deposited material, a heat-affected zone, and a substrate).

Steel 316L crystallizes first and, since it belongs to the austenitic class, it does not undergo phase transformations below the solidus point [34]. The ratio of the components in the entire temperature range for γ, $\alpha + \gamma$—phases corresponds to the values in Table 2. The quantitative analysis of other phases in the interface area was carried out according to the following algorithm.

At the first stage, according to the data in Table 3, the percentage content of the elements Fe, Al, Si was recalculated proceeding from the condition that their total content was 100%. Further, according to the diagram of the ternary state of Fe-Al-Si [35] (Figure 3) and Table 4, the possible composition of the phases of the system was determined.

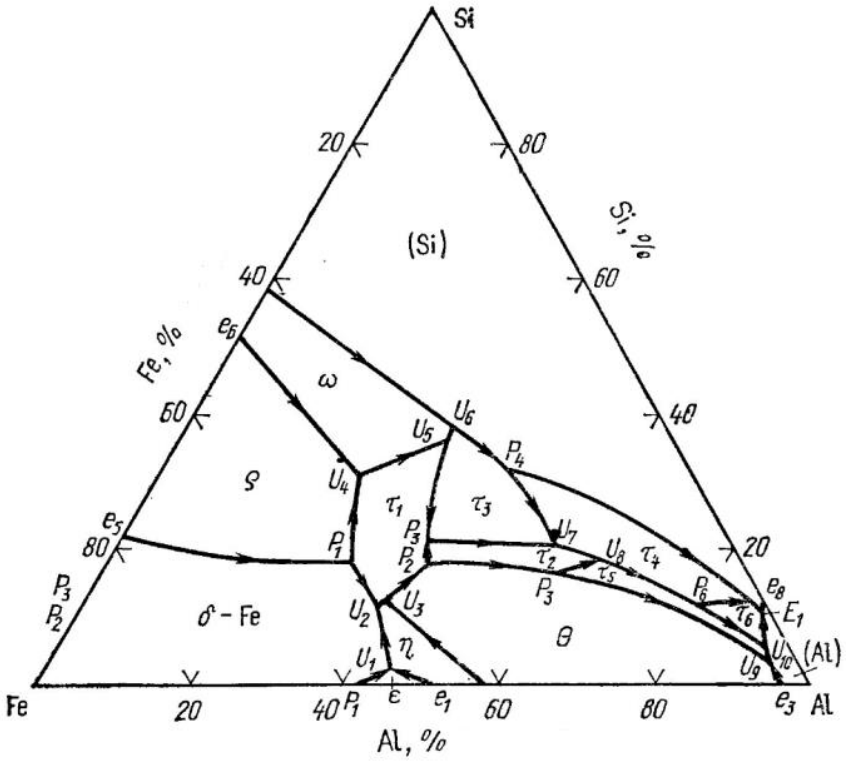

Figure 3. Fusibility diagram Fe-Al-Si (the percentage of elements is given by weight; τ_1—$Al_3Fe_3Si_2$; τ_2—$Al_{12}Fe_6Si_5$; τ_3—$Al_9Fe_5Si_5$; τ_4- Al_3FeSi_2; τ_5—$Al_{15}Fe_6Si_5$; τ_6—Al_4FeSi) data from [35].

In addition to the solid solution γ, $\alpha + \gamma$—phases of 316L, possible phases corresponding to the content of elements in Table 4 at the boundary of bimetal layers are presented in Table 5.

Table 5. Possible phases at the boundary of bimetal layers.

Place of Phase Separation	Phase Designation and Its Formula	Melting Temperature Range, °C	Invariant Reaction (See Figure 3)
From the side of 316L	$\tau_1(Al_3Fe_3Si_2)$, $\tau_2(Al_{12}Fe_6Si_5)$	935–940	$P_2 \rightarrow P_3$
From the side of AlSi10Mg	$\tau_5(Al_{15}Fe_6Si_5)$, $\tau_6(Al_4FeSi)$	615–620	U_9, U_{10}
	$(Al) + (Si)$	<577	E_1

At the second stage, the quantitative content of each phase from Table 5 and 316L phases was determined by the method of nonlinear programming. The problem of finding the content of phases in accordance with the law of mixtures is reduced to an optimization problem with linear constraints, which are presented in Tables 6 and 7. The variables x_i on the left side of the Tables 6 and 7 indicate the percentage of the *i*-phase. The coefficients for the variables x_i are the weight percentage of the element in the *i*-phase. The restrictions on the total content of each element in all phases for each sample are taken from Table 4. The content of each phase will be a solution to the inequality systems in Tables 6 and 7. The error of such calculations is residual $100 - \sum x_i$. The results of the quantitative analysis of the phase composition are presented in Table 8.

Table 6. The content of chemical elements in the phases from the side of the 316L substrate, at a distance of 20 μm from the interface zone.

Element	Sum of Element Content in All Phases, wt%	Content of Elements for Each SLM Scanning Mode, wt%				
		1	2	3	4	5
Fe	$55x_{Al3Fe3Si2} + 70.41x_{316L} + 0x_{(Al)+(Si)} \leq$	57.09	60.08	61.87	55.58	69.38
Al	$26.6x_{Al3Fe3Si2} + 0x_{316L} + (100 - C_{Si})x_{(Al)+(Si)} \leq$	18.34	14.19	12.78	19.73	2.86
Si	$18.4x_{Al3Fe3Si2} + 0x_{316L} + C_{Si}x_{(Al)+(Si)} =$	2.18	1.91	1.65	2.23	0.89
Cr	$0x_{Al3Fe3Si2} + 17.35x_{316L} + 0x_{(Al)+(Si)} \leq$	14.11	15.16	15.25	13.93	16.75
Ni	$0x_{Al3Fe3Si2} + 12.24x_{316L} + 0x_{(Al)+(Si)} \leq$	8.27	8.66	8.45	8.54	10.12
	$x_{Al3Fe3Si2} + x_{316L} + x_{(Al)+(Si)} \rightarrow 100$					

Table 7. The content of chemical elements in the phases from the side of the AlSi10Mg deposited layer, at a distance of 20 μm from the interface zone.

Element	Sum of Element Content in All Phases, wt%	Content of Elements for Each SLM Scanning Mode, wt%				
		1	2	3	4	5
Fe	$55x_{Al15Fe6Si5} + 29.1x_{Al4FeSi} + 70.41x_{316L} + 0x_{(Al)+(Si)} \leq$	57.09	60.08	61.87	55.58	69.38
Al	$46x_{Al15Fe6Si5} + 56.3x_{Al4FeSi} + 0x_{316L} + (100 - C_{Si})x_{(Al)+(Si)} \leq$	18.34	14.19	12.78	19.73	2.86
Si	$16x_{Al15Fe6Si5} + 14.6x_{Al4FeSi} + 0x_{316L} + C_{Si}x_{(Al)+(Si)} =$	2.18	1.91	1.65	2.23	0.89
Cr	$0x_{Al15Fe6Si5} + 0x_{Al4FeSi} + 17.35x_{316L} + 0x_{(Al)+(Si)} \leq$	14.11	15.16	15.25	13.93	16.75
Ni	$x_{Al15Fe6Si5} + 0x_{Al4FeSi} + 12.24x_{316L} + 0x_{(Al)+(Si)} \leq$	8.27	8.66	8.45	8.54	10.12
	$x_{Al15Fe6Si5} + x_{Al4FeSi} + x_{316L} + x_{(Al)+(Si)} \rightarrow 100$					

Table 8. Phase composition in the interface area of the bimetallic compound layers.

Location	Phase Content, wt%					
	$\tau_1(Al_3Fe_3Si_2)$	$\tau_5(Al_{15}Fe_6Si_5)$	$\tau_6(Al_4FeSi)$	γ, α + γ	(Al)+(Si)	Sum
SLM scanning mode 1						
From 316L side	11.85	-	-	67.57	15.19	94.61
From AlSi10Mg side	-	18.72	14.77	-	63.00	96.49
SLM scanning mode 2						
From 316L side	10.38	-	-	70.75	11.40	92.53
From AlSi10Mg side	-	6.07	8.75	-	82.00	96.82
SLM scanning mode 3						
From 316L side	8.97	-	-	80.87	10.02	99.86
From AlSi10Mg side	-	5.87	9.37	1.25	72.00	91.49
SLM scanning mode 4						
From 316L side	11.73	-	-	69.77	18.00	99.5
From AlSi10Mg side	-	17.75	10.06	38.91	26.62	93.34
SLM scanning mode 5						
From 316L side	4.84	-	-	89.87	1.57	96.28
From AlSi10Mg side	-	10.44	-	82.52	5.76	98.72

In the interface area of the grown bimetallic samples, tensile stresses were additionally created, which promote delamination by blowing metal balls onto the upper layer. The view of the samples after blowing is presented in Figure 4.

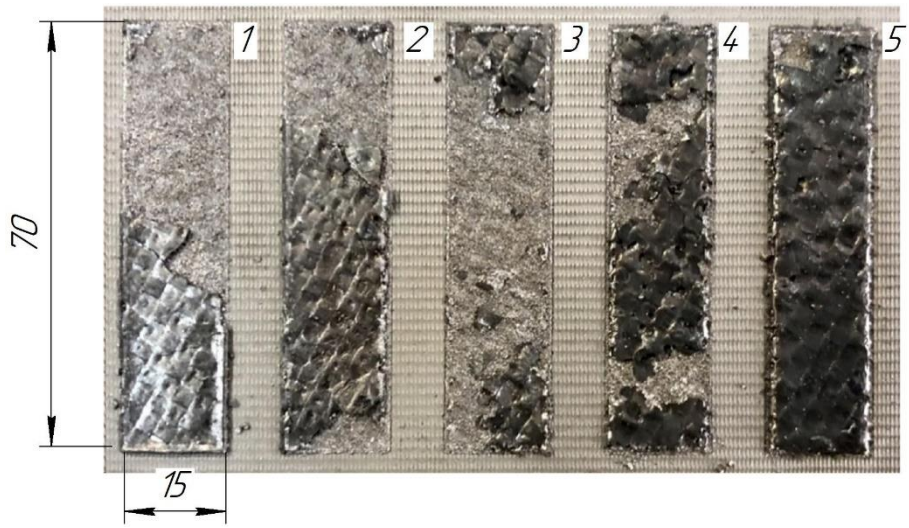

Figure 4. Delamination of samples after blowing (the keys correspond to SLM scanning mode).

4.2. Calculation of the Consolidation Criteria

The results of calculations of the heat capacities and consolidation criteria according to Equations (1)–(8) are summarized in Table 9.

Table 9. Criteria for consolidation at the interface.

Location	c_Ω, J/(mol·K)	c_σ, J/(mol·K)	k	K_1	K_2
SLM scanning mode 1					
From 316L side	73.213	76.344	0.959	0.993	0.604
From AlSi10Mg side	32.928	35.947	0.916		
SLM scanning mode 2					
From 316L side	85.662	88.974	0.963	0.973	0.548
From AlSi10Mg side	26.942	29.462	0.914		
SLM scanning mode 3					
From 316L side	96.090	99.520	0.966	0.969	0.518
From AlSi10Mg side	27.657	30.223	0.915		
SLM scanning mode 4					
From 316L side	67.969	71.001	0.957	1.088	0.724
From AlSi10Mg side	55.259	59.076	0.935		
SLM scanning mode 5					
From 316L side	190.227	194.936	0.976	1.018	0.701
From AlSi10Mg side	135.418	140.433	0.964		

For further analysis, let us determine the deviations of the calculated values of the consolidation criteria from Table 9 from their ideal values equal to 1:

$$\delta_i = |1 - K_i|. \quad (9)$$

Deviations of the criteria from the ideal value (the smaller the deviation is, the better it is) are presented in Figure 5.

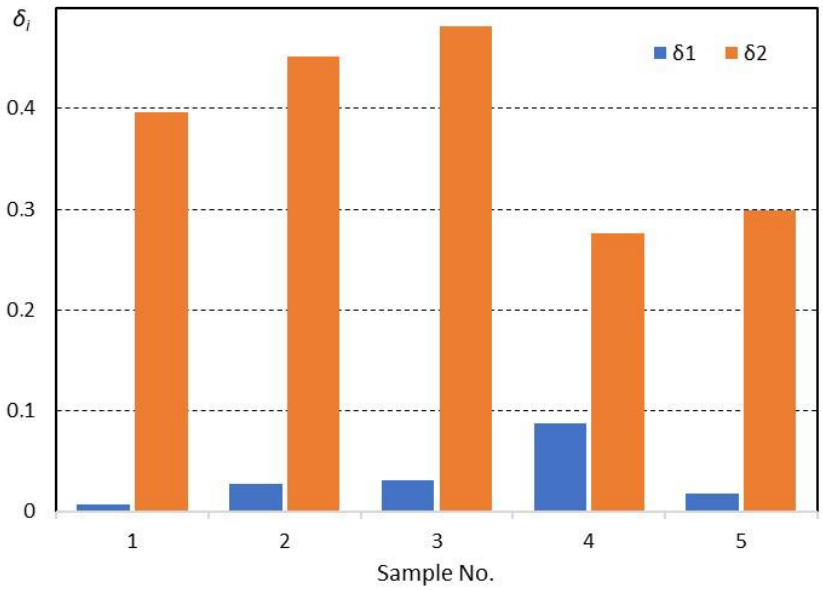

Figure 5. Deviations of the values of the thermodynamic criteria of consolidation from the ideal value for five samples.

The criteria for the SLM scanning mode 5 turned out to be closest to the ideal value. If we refer to Figure 4, with photographs of delamination of samples subjected to mechanical stress, we can note a qualitative similarity between the picture of delamination and the values of the consolidation criteria. Comparing the values of the consolidation criteria and the magnitude of their discrepancy with the desired values (Figure 5) with the delamination of the samples (Figure 4), it can be noted: (i) the most informative criterion for consolidation, reflecting the destruction, is the criterion (2), and (ii) the values of the consolidation criteria do not correlate with each other.

It should also be noted that the values of the consolidation criteria for each specific case do not yet serve as indicators of destruction; however, their significant deviation from 1 by more than 25–30%, as the studies demonstrate, indicate an increased likelihood of delamination.

5. Conclusions

The calculation results of the consolidation criteria (1) and (2), according to the methodology and dependencies outlined in Section 2, are presented. The proposed criteria should be used to determine the probability of cracking. The ideal values of the criteria are equal to 1. To determine the applicability of the proposed criteria, a series of experiments were carried out to create a bimetallic compound AlSi10Mg, steel 316L, by the method of selective laser melting with different energy densities of fusion. The results of the criteria calculations were compared with the results of the tests on adhesive strength and demonstrated an acceptable correlation with the test results. As demonstrated by the test results, the significant difference in the calculated criteria values by more than 25–30% from optimum designates an increased likelihood of delamination.

The consolidation criteria (1) and (2) do not at all pretend to fully reflect the physical phenomena occurring in the fusion area, even from the thermodynamic point of view. However, if the phase composition in the interface region is presumably known, then these criteria can serve as indicators of possible destruction.

Author Contributions: Conceptualization, A.K. and I.S.; methodology, V.S.; formal analysis, Y.E.; investigation, A.A. and V.R.; data curation, V.S. and Y.E.; writing—original draft preparation, A.K.; writing—review and editing, I.S.; visualization, V.R. All authors have read and agreed to the published version of the manuscript.

Funding: This research was funded by the Russian Science Foundation, grant number 20-69-46070.

Institutional Review Board Statement: Not applicable.

Informed Consent Statement: Not applicable.

Data Availability Statement: Not applicable.

Conflicts of Interest: The authors declare no conflict of interest.

References

1. Miyamoto, Y. *Functionally Graded Materials Design*; Processing and Applications Springer Science: New York, NY, USA, 1999.
2. Liyanage, T.; Kilbourne, J.; Gerlich, A.P.; North, T.H. Joint Formation in Dissimilar Al Alloy/Steel and Mg Alloy/Steel Friction Stir Spot Welds. *Sci. Technol. Weld. Join* **2009**, *14*, 500–508. [CrossRef]
3. Saleh, B.; Jiang, J.; Fathi, R.; Al-hababi, T.; Xu, Q.; Wang, L.; Song, D.; Ma, A. 30 Years of functionally graded materials: An overview of manufacturing methods. *Appl. Future Chall. Compos. Part B Eng.* **2020**, *201*, 108376. [CrossRef]
4. Yang, J.; Chen, J.; Zhao, W.; Zhang, P.; Yu, Z.; Li, Y.; Zeng, Z.; Zhou, N. Diode Laser Welding/Brazing of Aluminum Alloy to Steel Using a Nickel Coating. *Appl. Sci.* **2018**, *8*, 922. [CrossRef]
5. Olson, D.L.; Siewert, T.A.; Liu, S.; Edwards, G.R. *ASM Handbook: Volume 6. Welding, Brazing, and Soldering*, 10th ed.; ASM International: Novelty, OH, USA, 1993.
6. Trykov, Y.P.; Shmorgun, V.G.; Pronichev, D.V. *Methods for Studying the Structure and Properties of the Transition Zones of Explosion-Welded Metal*; Politekhnik: Volgograd, Russia, 2002.
7. Mehrpouya, M.; Gisario, A.; Barletta, M.; Natali, S.; Veniali, F. Dissimilar Laser Welding of NiTi Wires. *Lasers Manuf. Mater. Process* **2019**, *6*, 99–112. [CrossRef]
8. Tanaka, Y.; Kajihara, M. Kinetics of Isothermal Reactive Diffusion between Solid Fe and Liquid Al. *J. Mater. Sci.* **2010**, *45*, 5676–5684. [CrossRef]
9. Shishkovsky, I.V.; Nazarov, A.P.; Kotoban, D.V.; Kakovkina, N.G. Comparison of Additive Technologies For Gradient Aerospace Part Fabrication From Nickel Based Superalloys. In *Superalloys*; Aliofkhazraei, M., Ed.; IntechOpen: London, UK, 2015; pp. 221–245.
10. Shishkovsky, I.; Missemer, F.; Smurov, I. Direct metal deposition of functional graded structures in Ti-Al system. *Phys. Procedia* **2012**, *39*, 382–391. [CrossRef]
11. Shishkovsky, I.; Missemer, F.; Kakovkina, N.; Smurov, I. Intermetallics synthesis in the Fe–Al system via layer-by layer 3D laser cladding. *Crystals* **2013**, *3*, 517–529. [CrossRef]
12. Balzani, C.; Wagner, W.; Wilckens, D.; Degenhardt, R.; Busing, S.; Reimerdes, H.-G. Adhesive Joints in Composite Laminates—A Combined Numerical/Experimental Estimate of Critical Energy Release Rates. *Int. J. Adhes. Adhes.* **2012**, *32*, 23–38. [CrossRef]
13. Oyane, M.; Sato, T.; Okimoto, K.; Shima, S. Criteria for ductile fracture and their applications. *J. Mech. Work. Technol.* **1980**, *4*, 65–81. [CrossRef]
14. Clift, S.E.; Hartley, P.; Sturgess, C.E.N.; Rowe, G.W. Fracture prediction in plastic deformation processes. *Int. J. Mech. Sci.* **1990**, *32*, 1–17. [CrossRef]
15. Ko, Y.; Lee, J.; Huh, H.; Kim, H.; Park, S. Prediction of fracture in hub-hole expanding process using a new ductile fracture criterion. *J. Mater. Process. Technol.* **2007**, *187–188*, 358–362. [CrossRef]
16. Lou, Y.; Huh, H.; Lim, S.; Pack, K. New ductile fracture criterion for prediction of fracture forming limit diagrams of sheet metals. *Int. J. Solids Struct.* **2012**, *49*, 3605–3615. [CrossRef]
17. Liebowitz, H. *Fracture-An Advanced Treatise, Vol. II, Mathematical Fundamentals*; Pergamon Press: Oxford, UK, 1968.
18. Kinloch, A.; Wang, Y.; Williams, J.; Yayla, P. The mixed-mode delamination of fibre composite materials. *Compos. Sci. Technol.* **1993**, *47*, 225–237. [CrossRef]
19. Reeder, J.R. *An Evaluation of Mixed-Mode Delamination Failure Criteria*; Technical Memorandum TM-1992-104210; NASA, Langley Research Center: Hampton, VA, USA, 1992.
20. Balzani, C.; Wagner, W. An interface element for the simulation of delamination in unidirectional fiber-reinforced composite laminates. *Eng. Fract. Mech.* **2008**, *75*, 2597–2615. [CrossRef]
21. Rose, J.H.; Ferrante, J.; Smith, J.R. Universal Binding Energy Curves for Metals and Bimetallic Interfaces. *Phys. Rev. Lett.* **1981**, *47*, 675–678. [CrossRef]
22. Khaimovich, A.I.; Abulhanov, S.R. Equations of state of plastically deformed polycrystalline medium considering plastic deformation thermal effect. *ARPN J. Eng. Appl. Sci.* **2014**, *9*, 2867–2875.
23. Landau, L.D.; Lifshits, E.M. Statistical Physics. Part 1. In *Theoretical Physics*; Fizmatlit: Moscow, Russia, 2005.
24. Moracheskij, A.G.; Sladkov, I.B. *Thermodynamic Calculations in Metallurgy*; Metallurgiya: Moscow, Russia, 1985.
25. Leitner, J.; Voňka, P.; Sedmidubský, D.; Svoboda, P. Application of Neumann–Kopp rule for the estimation of heat capacity of mixed oxides. *Thermochim. Acta* **2010**, *497*, 7–13. [CrossRef]
26. Voight, W. Ueber die Beziehung zwischen den beiden Elasticitätsconstanten isotroper Körper. *Wied. Ann.* **1889**, *38*, 573–587. [CrossRef]

27. Karch, C. Micromechanical Analysis of Thermal Expansion Coefficients Modeling and Numerical. *Simul. Mater. Sci.* **2014**, *4*, 104–118.
28. Kerner, E.H. The Elastic and Thermo-elastic Properties of Composite Media. *Proc. Phys. Soc. B* **1956**, *69*, 808. [CrossRef]
29. Wakashima, K.; Tsukamoto, H. A Unified Micromechanical Approach toward Thermomechanical Tailoring of Metal Matrix Composites. *ISIJ Int.* **1992**, *32*, 883–892. [CrossRef]
30. Nigmatulin, R.I. *Fundamentals of Mechanics of Heterogeneous Media*; Nauka: Moscow, Russia, 1978.
31. Lupis, K. *Chemical Thermodynamics of Materials*; Metallurgia: Moscow, Russia, 1983.
32. Truesdell, C.; Toupin, R. The Classical Field Theories. In *Principles of Classical Mechanics and Field Theory. Encyclopedia of Physics*; Flügge, S., Ed.; Springer: Berlin, Germany, 1960; Volume 3. [CrossRef]
33. Khaimovich, A.; Erisov, Y.; Smelov, V.; Agapovichev, A.; Petrov, I.; Razhivin, V.; Bobrovskij, I.; Kokareva, V.; Kuzin, A. Interface Quality Indices of Al–10Si–Mg Aluminum Alloy and Cr18–Ni10–Ti Stainless-Steel Bimetal Fabricated via Selective Laser Melting. *Metals* **2021**, *11*, 172. [CrossRef]
34. Rivling, V.G.; Raynor, G.V. Critical evaluation of constitution of chromium-iron-nickel system. *Int. Met. Rev.* **1980**, *1*, 21–38.
35. Bannykh, O.A.; Budberg, P.B.; Alisova, S.P. *State Diagrams of Binary and Multicomponent Systems Based on Iron*; Bannykh, O.A., Dritsa, M.E., Eds.; Metallurgy: Moscow, Russia, 1986.